J Solid State Electrochem (2010) 14:923–930
DOI 10.1007/s10008-009-0883-5

ORIGINAL PAPER

Direct electrochemistry of myoglobin immobilized on chitosan-wrapped rod-constructed ZnO microspheres and its application to hydrogen peroxide biosensing

Xiumei Feng · Yuying Liu · Qingcheng Kong · Jianshan Ye · Xiaohua Chen · Jianqiang Hu · Zhiwu Chen

Received: 25 March 2009 / Revised: 25 May 2009 / Accepted: 6 June 2009 / Published online: 25 June 2009

Abstract Rod-constructed zinc oxide (ZnO) microspheres (RZnOMs), consisting of hundreds of needle-like ZnO nanorods, were utilized to explore a novel biosensor through coupling with myoglobin (Mb) in the presence of chitosan (Chi). Biocompatibility and electrochemical properties of the resulting ZnO-Chi-Mb composite film were studied by Fourier-transform infrared spectroscopy and cyclic voltammetry. The results revealed that the RZnOMs-based composite was a satisfying matrix for proteins to effectively retain their native structure and bioactivity. With advantages of the unique inorganic material, facilitated direct electron transfer of the metalloenzymes was acquired on the RZnOMs-based enzyme electrode. Moreover, the RZnOMs-based biosensor also displayed significant electrocatalytic activity for the reduction of hydrogen peroxide with an apparent Michaelis–Menten constant (32 μM), wide linear range (2–490 μM), and low detection limit (0.21 μM, S/N=3). These indicated that the RZnOMs were one of the ideal candidate materials for direct electrochemistry of redox proteins and related biosensor construction.

X. Feng · Y. Liu · Q. Kong · J. Ye · X. Chen · J. Hu
College of Chemistry and Chemical Engineering,
South China University of Technology,
Guangzhou 510640, People's Republic of China

Z. Chen
College of Materials Science and Engineering,
South China University of Technology,
Guangzhou 510640, People's Republic of China

J. Hu (✉) · Z. Chen
Key Laboratory of Low-Dimensional Materials & Application Technology of the Ministry of Education, Xiangtan University,
Xiangtan 411105, People's Republic of China
e-mail: jqhusc@scut.edu.cn

Keywords Zinc oxide microsphere · Biosensor · Direct electrochemistry · Electrocatalysis · Myoglobin · Hydrogen peroxide

Introduction

Nanomaterial-based biosensors and their direct electrochemistry have attracted an increased attention because many nanomaterials cannot only effectively retain enzyme bioactivity in the corresponding biosensors but greatly facilitate direct electron transfer between the enzymes and the underlying electrodes [1–4]. It is well known that good biocompatibility, strong stability, and high sensitivity are of key importance for electrochemical biosensors to offer effective electron transfer channels between redox-active enzymes and electrodes [5]. To improve biosensing electrochemical properties, great efforts have been done through tailoring the component, structure, size, and shape of nanomaterials possessing different electrochemical properties [6–9]. Metal oxide nanomaterials are an ideal candidate for the construction of the enzyme biosensors with high performance [10–13]. Among metal oxides, zinc oxide (ZnO), one of the important semiconductors in II–VI group, has been attracting considerable interest because of its combined properties of high surface area, nontoxicity, good biocompatibility, easy fabrication, plentiful oxygen vacancies, optical transparency, chemical and photochemical stability, and good electrocatalytic activity [14, 15]. At present, a series of newly shaped ZnO nanomaterials such as porous nanosheets [16], nanoflowers [17], and tetragonal pyramid-shaped porous nanostructures [18] have been synthesized and successfully applied to immobilize heme proteins and realize their direct electrochemistry. But, one-dimensional (1D) ZnO

nanomaterials should be the most promising to be utilized to construct biosensors with excellent biosensing properties and wide biological and medical applications because 1D nanomaterials can provide an efficient electron-conducting tunnel [19–21]. Therefore, rod-constructed ZnO microspheres (RZnOMs) are reasonably inferred to possess good electron-conducting capability, and their corresponding biosensors have better electrochemical performance and wider applications in comparison with those fabricated by 1D or other shape ZnO nanomaterials.

Myoglobin (Mb) is a single-chain heme protein whose physiological importance is principally related to its ability to bind molecular oxygen (O_2). It plays an important role in O_2 transport from the periphery of animal cell to the mitochondria [22, 23]. It is also an ideal model to study direct electrochemistry, biological sensing, and electrocatalysis of heme proteins because bioactive Mb immobilized on an electrode surface usually exhibits good electrocatalytic activity for O_2, hydrogen peroxide (H_2O_2), trichloroacetic acid, nitrite, etc. [24]. However, it is difficult for proteins to realize direct electron transfer on "bare" electrodes because of their easy denaturation, deeply embedded active centers, impurity adsorption, and often unfavorable orientations [25, 26]. To date, great efforts have, thus, been made to improve the sensitivity of Mb-based biosensors for the detection of some important and trace molecules such as H_2O_2. H_2O_2 is not only by-product generated from many biological oxidase reactions but also an ideal target molecule to analyze and detect food, clinical, pharmaceutical, industrial, and environment [24]. Therefore, it is very important to design a sensitive method for rapid, accurate, and reliable determination of H_2O_2 with wide linear range.

In the present study, RZnOMs, consisting of hundreds of needle-like ZnO nanorods, were prepared by a hydrothermally synthetic route. And that the RZnOMs were for the first time explored to fabricate a novel hydrogen peroxide biosensor through entrapping Mb in the presence of chitosan (Chi). As an inorganic–organic hybrid material, the ZnO-Chi-Mb composite could effectively maintain the native structure of Mb and facilitated direct electron transfer of Mb has been achieved. The constructed biosensor was also successfully employed for the detection of H_2O_2 and displayed good electrochemical performance.

Materials and methods

Materials

Myoglobin (MW 18800) was purchased from Yuanju Biology Science and Technology Co. Ltd (Shanghai, China), and Chi came from Aldrich. The following analytical reagent-grade reagents were obtained from Guangdong Guanghua Chemical Reagent Co.: zinc nitrate ($Zn(NO_3)_2{\cdot}6H_2O$), sodium hydroxide (NaOH), cetyltrimethyl ammonium bromide (CTAB), sodium dihydrogen phosphate (NaH_2PO_4), disodium hydrogen phosphate (Na_2HPO_4), phosphoric acid (H_3PO_4), hydrogen peroxide (H_2O_2), concentrated hydrochloric acid (HCl), concentrated nitric acid (HNO_3), and high-purity nitrogen. All above reagents were used without further purification. Milli-Q water (>18.0 MΩ cm) was used to prepare all aqueous solutions. All glassware used was washed with aqua regia and rinsed with >18.0 MΩ cm water prior to use; 20 mM of phosphate buffer solution (PBS, pH 7.0) was prepared by mixing 39 mL 20 mM NaH_2PO_4 and 61 mL 20 mM Na_2HPO_4, and then various pH values of PBS were obtained through adjusting the PBS pH with a small quantity of 0.1 M H_3PO_4 or NaOH solutions.

Synthesis of RZnOMs

In a typical procedure for the synthesis of RZnOMs, 30 mL of $Zn(OH)_4^{2-}$ solution was first prepared by dissolving 10 mmol $Zn(NO_3)_2{\cdot}6H_2O$ and 100 mmol NaOH in 30 mL milli-Q water. Then, 36 mL of 10% CTAB was introduced to the as-prepared solution, and the mixture was stirred for 30 min. Finally, the mixture was put into a 100-mL Teflon-lined stainless-steel autoclave, and the autoclave was heated at 120 °C for 3 h. The final product was obtained by repeatedly washing the sediment with milli-Q water and ethanol and drying at 60 °C for 4 h.

Preparation of modified electrodes

Three-millimeter diameter glassy carbon (GC) electrode was polished with alumina (Al_2O_3) slurry of successively smaller particles (1.0-, 0.3-, and 0.05-μm diameters), respectively. Then, the electrode was cleaned by ultrasonication in ultrapure water and ethanol, respectively. In a typical procedure for the preparation of ZnO-Chi-Mb-modified electrode, 10 mg RZnOMs and 50 mg Chi was first dispersed in 10 ml 2% acetic acid solution, and then the mixture was stirred and ultrasonically dispersed for 1.5 h (solution I). Second, solution I was mixed with 8 mg/mL Mb dissolved in 20 mM pH 7.0 PBS according to the ratio of 1:1 (*v*/*v*) (solution II). At last, 3 μL of solution II was cast on the surface of the polished GC electrode. A beaker was covered over the electrode so that water could evaporate slowly in air and a uniform film electrode could be formed. The modified electrode was stored at 4 °C in a refrigerator when not in use. Similarly, Chi-Mb- and ZnO-Chi-modified GC electrodes were also prepared.

Apparatus and measurements

Transmission electron microscopy (TEM) was performed with a Hitachi H-7500 microscope operated at 80 kV. Scanning electron microscopy (SEM) and energy-dispersive X-ray spectroscopy (EDS) were carried out with a field-emission microscope (LEO, 1530 VP) operated at an accelerating voltage of 30 kV. X-ray diffraction (XRD) pattern was recorded on a powder sample using a D/max-IIIA (Japan) X-ray diffractometer with graphite monochromatized Cu Kα radiation (λ= 0.15418 nm) in ranging from 10° to 80°. Fourier-transform infrared (FTIR) spectra were obtained on Tensor 27 (Bruker Company, German). The FTIR samples were prepared according to the following procedure: ZnO-Chi-Mb, Chi-Mb, or Mb solutions were first cast onto three glass slides, respectively. Then, the glass slides were naturally dried in air. Finally, the dry films adhered to the glass slides were stripped off and tableted with KBr powders for FTIR measurements.

Electrochemical measurements were performed at room temperature using a CHI660 electrochemical workstation (CH Instru. Co., Shanghai, China). The measurements were based on a three-electrode system with the as-prepared film electrode as the working electrode, a platinum wire as the auxiliary electrode, and a saturated Ag/AgCl electrode as the reference electrode. Without special statement, 20 mM pH 7.0 PBS was used as the electrolyte in all experiments.

Results and discussion

Morphology and crystalline structure characterization of RZnOMs

Figure 1 gives typical TEM and SEM images of RZnOMs prepared using a hydrothermally synthetic route. The TEM and SEM images showed a clear view of its 3D stereographic structure. The RZnOMs possessed a well-defined shape with the average diameter of about 5.5 μm, which consisted of hundreds of needle-like ZnO nanorods. The needle-like ZnO nanorods had an average length of about 3 μm and tapered diameters from around 150 nm to around 60 nm. Such structure not only offered higher surface area but also had numerous active sites (e.g., the tips of the needle-like ZnO nanorods and their forming cavities), which were much useful to fix enzyme and protein on the surface. To verify the component of the RZnOMs produced, EDS measurement was, thus, preformed. The Cu, C, Au, and Pd elements observed in the Fig. 1d were from the copper grids and spurted Au–Pd alloy made for the SEM sample. The appearance of two elements of Zn and O could infer that the sample produced using the present method was perhaps ZnO microspheres.

Figure 2 shows XRD pattern of RZnOMs prepared using the present method. The data displayed diffraction peaks at 2θ=31.8°, 34.4°, 36.2°, 47.5°, 56.6°, 62.8°, 66.4°, 67.9°, 69.1°, 72.6°, and 76.9°, which could be indexed to (100), (002), (101), (102), (110), (103), (200), (112), (201), (004), and (202) planes of the hexagonal wurtzite structure of zinc

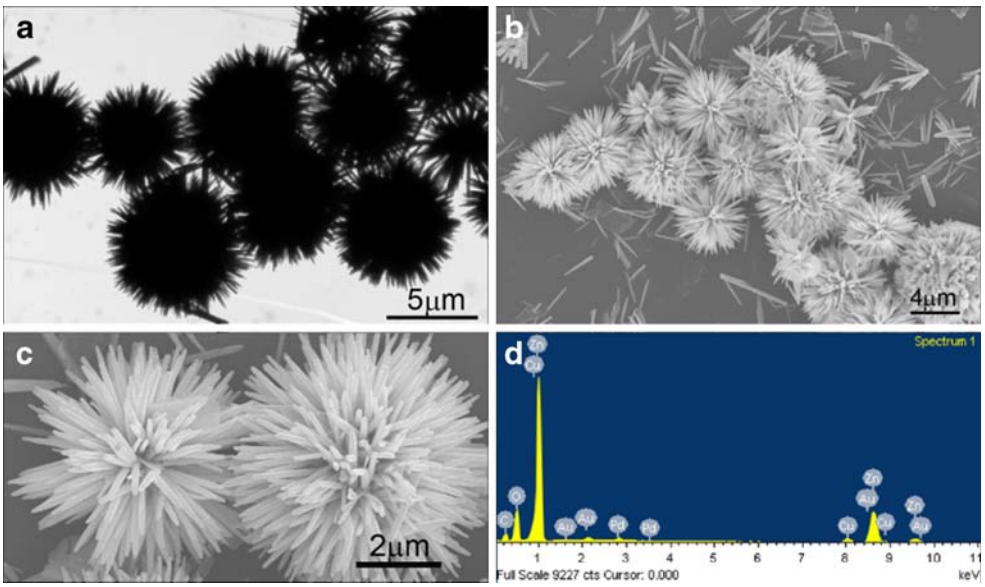

Fig. 1 **a** TEM and **b**, **c** SEM images, and **d** EDS spectrum of rod-constructed ZnO microspheres prepared by the present method, respectively. *Scale bar* **a** 5 μm and **b**, **c** 2 μm

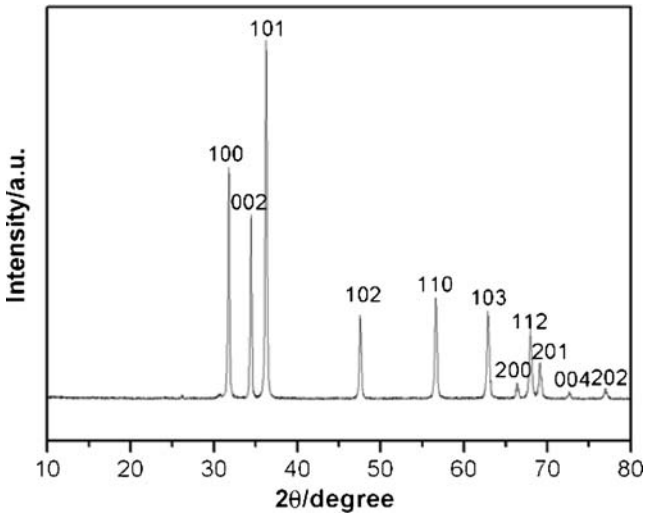

Fig. 2 XRD pattern of rod-constructed ZnO microspheres prepared using the present method

oxide (JCPDS: 80-0075, space group: *P*63*mc*), respectively. No characteristic peaks of other compounds such as zinc hydroxide ($Zn(OH)_2$) was observed, indicating that the sample produced, thus, was pure ZnO. Moreover, the sharp diffraction peaks revealed that the as-prepared sample had a good crystallinity.

Spectroscopic characterization of ZnO-Chi-Mb composite film

Previous studies have confirmed that FTIR spectroscopy is an effective means to probe into the secondary structure of proteins [27, 28]. Figure 3 displays FTIR spectra of dry Mb, Chi-Mb, and ZnO-Chi-Mb films. Characteristic FTIR peaks at approximately 1,658 and 1,540 cm^{-1} (curve a) could be ascribed to the spectra of amide I (1,700–1,600 cm^{-1}) and amide II (1,620–1,500 cm^{-1}) bands of native Mb, respectively [29]. As shown in Fig. 3, when Mb was entrapped in the Chi and ZnO-Chi films, the Mb spectrum peaks at the Chi-Mb (curve b, 1,658 and 1,543 cm^{-1}) and ZnO-Chi-Mb (curve c, 1,655 and 1,543 cm^{-1}) composite films were nearly the same with those at native Mb. The similarities of the three spectra suggested that Mb retained the essential features of its native secondary structure in ZnO-Chi-Mb and Mb-Chi composite films.

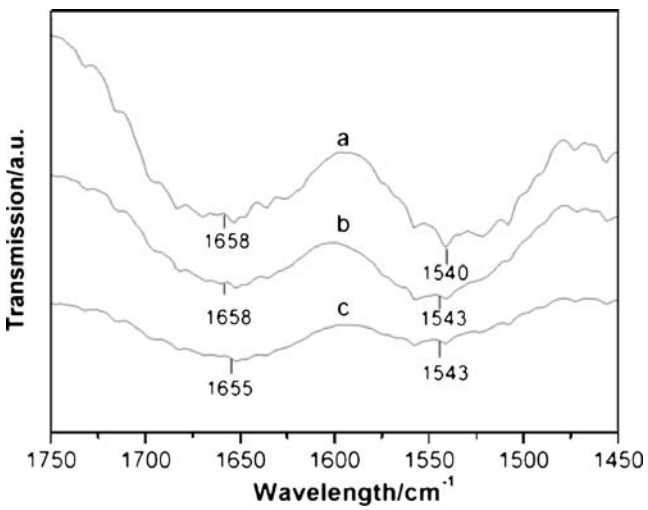

Fig. 3 FTIR spectra of **a** Mb, **b** Chi-Mb, and **c** ZnO-Chi-Mb dry films

Direct electrochemistry of the immobilized Mb

Figure 4 shows typical cyclic voltammograms of GC electrodes modified with ZnO-Chi, Chi-Mb, and ZnO-Chi-Mb in 20 mM PBS with scan rate of 0.20 V/s. It was clearly seen from Fig. 4a that no redox peak appeared at the ZnO-Chi-modified electrode, indicating that the RZnOMs were not an electroactive material in the potential range. However, a pair of stable, quasi-reversible, well-defined, and relatively weak peaks for Mb-Fe^{III}/Fe^{II} redox couple could be observed at the Chi-Mb electrode (Fig. 4b), which could be contributed to the direct electron transfer between the Mb and the underlying electrode [30]. When the RZnOMs were introduced into the Chi-Mb composite system, the redox current of the ZnO-Chi-Mb-modified electrode was significantly enhanced (Fig. 4c), which was about 5-fold larger than that of the Mb-Chi modified electrode. The great enhancement indicated that the RZnOMs played a key role in facilitating the electron transfer between the Mb and the underlying electrode. The increased electrochemical performance of the ZnO-Chi-Mb film could be perhaps clarified according the following three aspects. First, as above-mentioned, the good biocompatibility of the ZnO-Chi-Mb composite may prevent denaturation and retain the essential secondary structure of

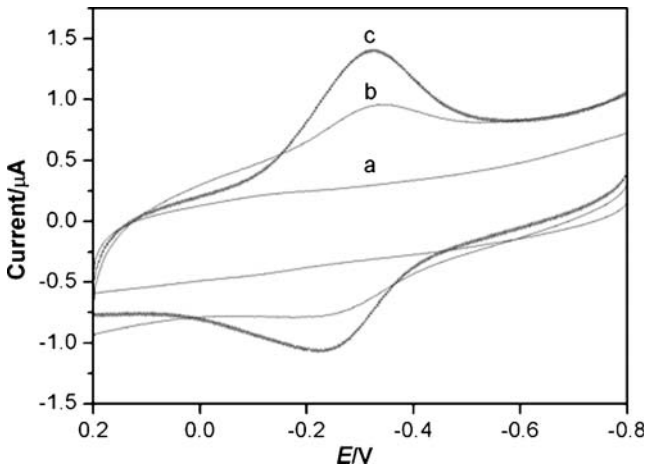

Fig. 4 Cyclic voltammograms of different modified electrodes in 20 mM pH 7.0 PBS. **a** Chi/GC, **b** Chi-Mb/GC, and **c** ZnO-Chi-Mb/GC. Scan rate=0.20 V/s

the entrapped Mb. Second, the high chemical activity of the nanorods' tips and cavities between the nanorods in the ZnO microspheres may be available to bind Mb and provide an efficient electron-conducting tunnel [20]. Finally, the rod-constructed microstructure may serve as a rigid framework to favor the appropriate conformation of the entrapped Mb. The formal potential (estimated as $(E_{pa}+E_{pc})/2$, where E_{pa} and E_{pc} are the anodic and cathodic peak potentials, respectively) of Mb was found to be about −0.28 V, characteristic of Mb-Fe^{III}/Fe^{II} redox couple in various films [31–33]. The peak-to-peak potential separation (ΔEp) directly related to the electron transfer was found to be about 66 mV, which is smaller than that (about 91 mV) of the Chi-Mb-modified electrode. The smaller ΔEp revealed that the Mb on the ZnO-Chi-Mb electrode possessed a fast and quasi-reversible electron transfer process. By integrating the cathodic peak in Fig. 4c, the average surface concentration (Γ^*) of electroactive Mb in the ZnO-Chi-Mb film was estimated to be about 1.3×10^{-10} mol cm^{-2} according to Faraday's law $Q=nFA\Gamma^*$ (where F is the Faraday constant, Q can be obtained by integrating the cathodic peak of the Mb, and n and A stand for the number of electron transferred and the effective area of the electrode, respectively), which was higher than the reported value (3.7×10^{-11} mol cm^{-2}) [34]. The value obtained in our experiment indicated that only those Mb molecules in the inner layers of the films closest to the electrodes and with a suitable orientation could exchange electrons with the underlying electrode.

Figure 5 gives typical cyclic voltammograms of the ZnO-Chi-Mb-modified electrode with scan rates from 0.1 to 1.0 V s^{-1}. With the increase of the scan rates, the cathodic and anodic peak currents of Mb increased simultaneously, as shown in the inset of Fig. 5, and the cathodic and anodic peak currents increased linearly with scan rates from 0.1 to 1.0 V s^{-1}. This revealed that the electron transfer between the Mb and the underlying electrode could be easily performed at the ZnO-Chi-Mb composite film and it was a surface-controlled electrochemical process. According to the Laviron method [35], the heterogeneous electron transfer rate constant (k_s) of the Mb immobilized on the ZnO-Chi-Mb-modified electrode was estimated to be 6.20±1.11 s^{-1}, which is higher than that on Chi-Mb-modified electrode (2.71±0.85 s^{-1}).

Figure 6 displays typical cyclic voltammograms of ZnO-Chi-Mb-modified electrode measured with different pH values at 0.2 V/s. It was found that the direct electrochem-

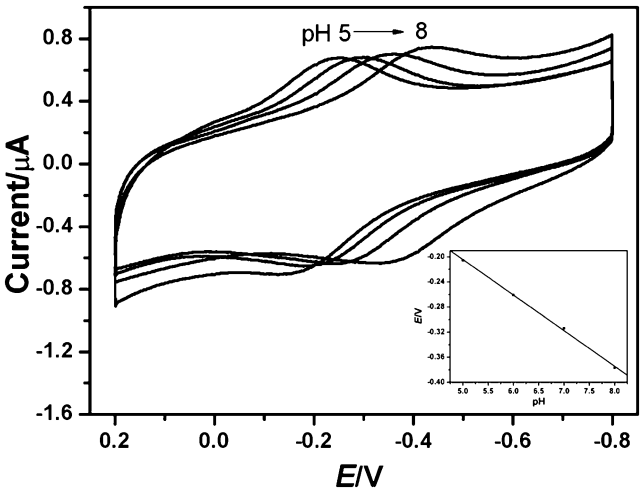

Fig. 6 Cyclic voltammograms of ZnO-Chi-Mb-modified electrode measured with different pH values at 0.2 V/s. *Inset* calibration plot of the apparent formal potential versus pH values

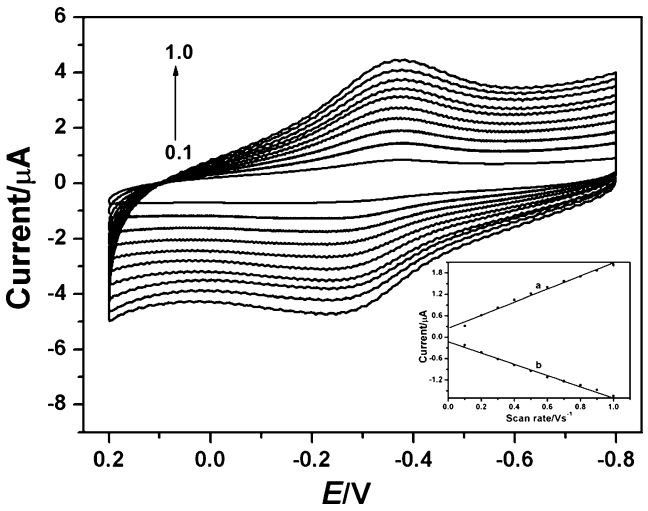

Fig. 5 Cyclic voltammograms of ZnO-Chi-Mb-modified electrode measured with different scan rates: from 0.1 to 1.0 V/s. *Inset* calibration plot of cathodic (curve *a*) and anodic (curve *b*) peak currents vs. scan rates

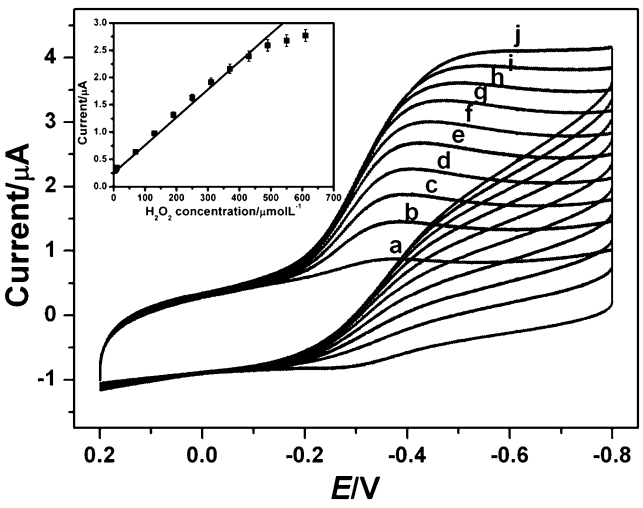

Fig. 7 Electrocatalysis of H_2O_2 at ZnO-Chi-Mb-modified electrode with H_2O_2 concentrations of **a** 0, **b** 70, **c** 130, **d** 190, **e** 250, **f** 310, **g** 370, **h** 430, **i** 490, and **j** 550 μM, respectively. Scan rate: 0.2 V/s. *Inset* calibration plot of cathodic peak currents vs. H_2O_2 concentrations

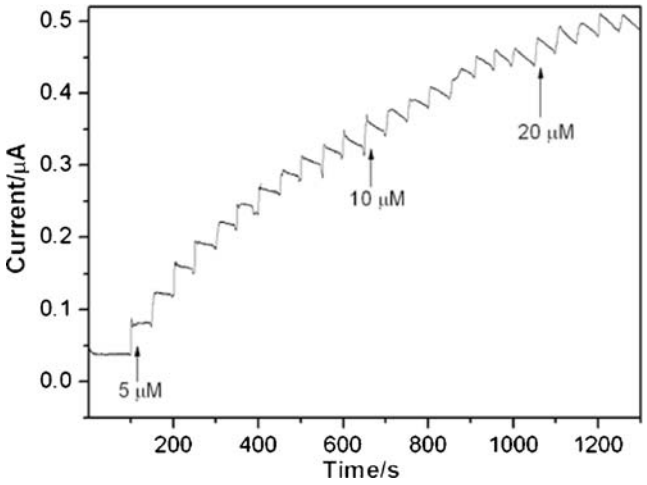

Fig. 8 Typical current–time response curves of the ZnO-Chi-Mb biosensor upon successive addition of H_2O_2 into pH 7.0 PBS. Applied potential=−0.32 V (vs. Ag/AgCl)

istry of the ZnO-Chi-Mb-modified electrode intimately depended on solution pH. When the solution pH increased from 5 to 8, both the reduction and oxidation peaks linearly shifted to the negative (the inset of Fig. 6). It was reversible for these voltammetric peak potentials switched among different pH values. The slope calculated from the linear plot of *E*p versus pH was about −57.0 mV pH^{-1}, which was close to the expected value of −58.0 mV pH^{-1} [36]. This indicated that a single proton transfer coupled to the single electron transfer in order to neutralize the excess charge on the electrochemical interface.

Electrocatalytic properties of the biosensor for H_2O_2 determination

Electrocatalytic activity of the ZnO-Chi-Mb-modified electrode toward H_2O_2 was examined by cyclic voltammograms (Fig. 7). When H_2O_2 was added to blank PBS, a significant increase in the cathodic (reduction) peak current at about −0.32 V was observed accompanying the decrease of anodic (oxidation) peak current, suggesting a typical electrocatalytic reduction process of H_2O_2 by Mb in the ZnO-Chi-Mb film [23]. The possible mechanism of electrocatalytic reduction of H_2O_2 at the Mb-based enzyme electrode should be similar to that reported recently [37, 38], which can be expressed as follows:

$$Mb\left[Heme\left(Fe^{III}\right)\right] + e^- \rightarrow Mb\left[Heme\left(Fe^{II}\right)\right] \quad (1)$$

$$Mb\left[Heme\left(Fe^{II}\right)\right] + H_2O_2 + 2H^+ + e^- \rightarrow Mb\left[Heme\left(Fe^{III}\right)\right] + 2H_2O \quad (2)$$

The whole reaction would be:

$$H_2O_2 + 2H^+ + 2e^- \rightarrow 2H_2O \quad (3)$$

The cathodic peak current increased linearly with increasing H_2O_2 concentration, as shown in the inset of Fig. 7. The linear range was from 2 to 490 μM (R=0.9977, n=13), which was much wider than those reported in the Mb-based enzyme electrodes [25, 39]. Further increasing the H_2O_2 concentration (>490 μM), the catalytic current increased up to a limiting value whose saturation behavior was characteristic of enzyme-based catalysis. The detection limit was around 0.21 μM when the signal to noise ratio was 3. The sensitivity of the enzyme electrode was calculated to be about 74 mA cm^{-2} mol^{-1}, indicating that Mb entrapped in the composite film had excellent bioelectrocatalytic activity towards H_2O_2.

The amperometric response of the as-prepared biosensor for H_2O_2 was also investigated by amperometric current–time curve method. The electrocatalytic reduction peak potential (i.e., −0.32 V) was selected as the constant applied potential for the high sensitivity together with a wide linear range. With a stepwise increase of H_2O_2 concentration in the stirring PBS, the biosensor responded rapidly to the substrate and a stepwise growth of reduction current was observed, as shown in Fig. 8. The response time (achieving 95% of the steady-state current) was less than 5 s. Such a rapid response can be ascribed to the fast diffusion of the substrate in the RZnOMs composite film. The apparent Michaelis–Menten constant (K_m), an indication of the enzyme-substrate kinetics, was estimated to be about 32 μM according to the electrochemical version of Lineweaver–Burk equation [40]. The value obtained from the ZnO-Chi-Mb composite film was smaller than those of

Table 1 Comparison of the electrocatalytic properties of different Mb-based-modified electrodes for H_2O_2 determination

Electrode	Line rang (μM)	Detection limit (μM)	K_m (μM)	k_s (s^{-1})	References
Mb/clay-IL/GCE	4–259	0.73	17.6	3.58±0.12	[17]
Mb-TiO_2/MWCNTs/GCE	1–42	0.41	83.1	3.08	[18]
Mb/ZrPNS/GCE	1–13	0.14	34.0	5.60	[30]
Mb-Zr$(UMP)_2$•H_2O/GCE	4–180	1.52	196.1	1.10±0.30	[41]
Mb-Chi-ZnO/GCE	2–490	0.21	32.0	6.02±1.11	This paper

other Mb-based matrices [11, 28, 41], suggesting that Mb entrapped in the composite film possessed high peroxidase-like activity. The high catalytic activity may result from the high chemical reaction activity and large surface area of the RZnOMs. For comparison with the Mb-based-modified electrodes reported previously, comparison of the electrocatalytic properties of different Mb-based-modified electrodes for H_2O_2 determination is listed in Table 1. It could be seen that the ZnO-Chi-Mb-modified electrode fabricated by the present method possessed excellent electrocatalytic performance for the determination of H_2O_2.

Reproducibility and stability of the biosensor

The electrode-to-electrode reproducibility of the biosensor was studied at seven different electrodes under the same conditions independently. The relative standard deviation of the seven biosensors response to 120 μM H_2O_2 was around 4%, indicating a good electrode-to-electrode reproducibility. The biosensor was measured two times by cyclic voltammogram when it was immersed in pH 7.0 PBS for the time interval of 4 h. The decrease of the cathodic peak current was less than 2% after 4 h, suggesting that the biosensor had a good stability. Additionally, the biosensor could retain 95% of its initial response after 10-day storage in pH 7.0 PBS, suggesting that the biosensor had an acceptable long-term stability. The good reproducibility and stability can be ascribed to the unique microstructure, shape, and good biocompatibility of the RZnOMs.

Conclusion

In summary, we have synthesized rod-constructed ZnO microspheres by a facile hydrothermal route. These unique ZnO nanomaterials that consisted of hundreds of needle-like ZnO nanorods were explored for constructing direct electrochemical biosensor and proved to be a good immobilization matrix for proteins and enzymes. The obtained results revealed that Mb entrapped in the composite film retained its essential secondary structure, and displayed a pair of quasi-reversible redox peaks at about −0.28 V in 20 mM pH 7.0 PBS. The biosensor also exhibited an excellent electrocatalytic activity and a fast amperometric response to H_2O_2 with wide linear range (2 to 490 μM) and low detection limit (0.21 μM), good reproducibility and stability, and good long-term stability. The relatively small K_m (about 32 μM) indicated that Mb entrapped in the composite film possessed high peroxidase-like activity. The rod-constructed ZnO microspheres have been proved to be a promising matrix for immobilizing enzymes and constructing electrochemical biosensors and are also expected to find potential applications in biomedical, food, and environmental analysis and detection.

Acknowledgements The work was financially supported by National Natural Science Foundation of China (Nos. 20773040, 50702022), The Research Fund for the Doctoral Program (New Young Teacher) of Higher Education (No. 20070561005), One Hundred Person Project of The South China University of Technology, and the Open Project Program of Low Dimensional Materials and Application Technology (Xiangtan University), Ministry of Education, China (Nos. KF0701, DWKF0803).

References

1. Wang J (2008) Chem Rev 108:814–825. doi:10.1021/cr068123a
2. Lu XB, Wen ZH, Li JH (2006) Biomaterials 27:5740–5747. doi:10.1016/j.biomaterials.2006.07.026
3. Deng CY, Chen JH, Chen XL, Xiao CH, Nie LH, Yao SZ (2008) Biosens Bioelectron 23:1272–1277. doi:10.1016/j.bios.2007.11.009
4. Jiang HJ, Du C, Zou ZQ, Li XW, Akins DL, Yang H (2009) J Solid State Electrochem 13:791–798. doi:10.1007/s10008-008-0612-5
5. Liu GZ, Paddon-Row MN, Gooding JJ (2007) Electrochem Commun 9:2218–2223. doi:10.1016/j.elecom.2007.06.016
6. Dai ZH, Liu K, Tang YW, Yang XD, Bao JC, Shen J (2008) J Mater Chem 18:1919–1926. doi:10.1039/b717794a
7. Ivnitski D, Artyushkova K, Rincón RA, Atanassov P, Luckarift HR, Johnson GR (2008) Small 4:357–364. doi:10.1002/smll.200700725
8. Feng XM, Hu JQ, Chen XH, Xie JS, Liu YY (2009) J Phys D Appl Phys 42:042001. doi:10.1088/0022-3727/42/4/042001
9. Chen XH, Hu JQ, Chen ZW, Feng XM, Li AQ (2009) Biosens Bioelectron (in press). doi:10.1016/j.bios.2009.04.037
10. Sheng QL, Luo K, Li L, Zheng JB (2009) Bioelectrochemistry 74:246–253. doi:10.1016/j.bioelechem.2008.08.007
11. Liu AH, Wei MD, Honma I, Zhou HS (2005) Anal Chem 77:8068–8074. doi:10.1021/ac051640t
12. Lee WJ, Smyrl WH (2005) Electrochem Solid-State Lett 8:B7–B9. doi:10.1149/1.1857115
13. Chen ZW, Yu Y, Guo H, Hu JQ (2009) J Phys D Appl Phys 42:125–307.
14. Topoglidis E, Cass AEG, O'Regan B, Durrant JR (2001) J Electroanal Chem 517:20–27. doi:10.1016/S0022-0728(01)00673-8
15. Zhu XL, Yuri I, Gan X, Suzuki I, Li GX (2007) Biosens Bioelectron 22:1600–1604. doi:10.1016/j.bios.2006.07.007
16. Lu XB, Zhang HJ, Ni YW, Zhang Q, Chen JP (2008) Biosens Bioelectron 24:93–98. doi:10.1016/j.bios.2008.03.025
17. Zhang YW, Zhang Y, Wang H, Yan BN, Shen GL, Yu RQ (2009) J Electroanal Chem 627:9–14. doi:10.1016/j.jelechem.2008.12.010
18. Dai ZH, Shao GJ, Hong JM, Bao JC, Shen J (2009) Biosens Bioelectron 24:1286–1291. doi:10.1016/j.bios.2008.07.047
19. Huynh WU, Dittmer JJ, Alivisatos AP (2002) Science 295:2425–2427. doi:10.1126/science.1069156
20. Wang JX, Sun XW, Wei A, Lei Y, Cai XP, Li CM, Dong ZL (2006) Appl Phys Lett 88:233106. doi:10.1063/1.2210078
21. Liu JP, Guo CX, Li CM, Li YY, Chi QB, Huang XT, Liao L, Yu T (2009) Electrochem Commun 11:202–205. doi:10.1016/j.elecom.2008.11.009
22. Dai Z, Xiao Y, Yu XZ, Mai ZB, Zhao XJ, Zou XY (2009) Biosens Bioelectron 24:1629–1634. doi:10.1016/j.bios.2008.08.032
23. Zhang L, Tian DB, Zhu JJ (2008) Bioelectrochemistry 74:157–163. doi:10.1016/j.bioelechem.2008.07.003

24. Zhao G, Xu JJ, Chen HY (2006) Anal Biochem 350:145–150. doi:10.1016/j.ab.2005.11.035
25. Hamachi I, Noda S, Kunitake T (1991) J Am Chem Soc 113:9625–9630. doi:10.1021/ja00025a031
26. Wang QL, Lu GX, Yang BJ (2004) Langmuir 20:1342–1347. doi:10.1021/la035321d
27. Krimm S, Bandekar J (1986) Adv Protein Chem 38:181–364. doi:10.1016/S0065-3233(08)60528-8
28. Dong AC, Huang P, Caughey WS (1990) Biochem 29:3303–3308. doi:10.1021/bi00465a022
29. Wang GX, Liu Y, Hu NF (2007) Electrochim Acta 53:2071–2079. doi:10.1016/j.electacta.2007.09.013
30. Zhang YH, Chen X, Yang WS (2008) Sens Actuat B 130:682–688. doi:10.1016/j.snb.2007.10.034
31. Zhang L, Zhang Q, Li JH (2007) Adv Funct Mater 17:1958–1965. doi:10.1002/adfm.200600991
32. Rusling JF, Nassar AEF (1993) J Am Chem Soc 115:11891–11897. doi:10.1021/ja00078a030
33. Zhou YL, Hu NF, Zeng YH, Rusling JF (2002) Langmuir 18:211–219. doi:10.1021/la010834a
34. Zhao XJ, Mai ZB, Kang XH, Dai Z, Zou XY (2008) Electrochim Acta 53:4732–4739. doi:10.1016/j.electacta.2008.02.007
35. Laviron E (1979) J Electroanal Chem 101:19–28. doi:10.1016/S0022-0728(79)80075-3
36. Nassar AEF, Zhang Z, Hu NF, Rusling JF (1997) J Phys Chem B 101:2224–2231. doi:10.1021/jp962896t
37. Huang H, Hu NF, Zeng YH, Zhou G (2002) Anal Biochem 308:141–151. doi:10.1016/S0003-2697(02)00242-7
38. Lu XB, Hu JQ, Yao X, Wang ZP, Li JH (2006) Biomacromolecules 7:975–980. doi:10.1021/bm050933t
39. Wang F, Hu SS (2008) Colloids Surf B 63:262–268. doi:10.1016/j.colsurfb.2007.12.020
40. Kamin RA, Wilson GS (1980) Anal Chem 52:1198–1205. doi:10.1021/ac50058a010
41. Qiao YB, Jian FF, Bai Q (2008) Biosens Bioelectron 23:1244–1249. doi:10.1016/j.bios.2007.11.008